High Order Finite Difference Modal Method for Diffraction Gratings

Dawei Song and Ya Yan Lu

Department of Mathematics, City University of Hong Kong, Kowloon, Hong Kong

A new high order finite difference modal method (FDMM) is developed for analyzing diffraction gratings in conical and classical mountings. The difference scheme is constructed by enforcing the internal interface conditions in each grating layer to high order derivatives, and it gives a high order of accuracy for computing the eigenmodes of the grating layer. Between different layers, the interface conditions are implemented using a Fourier matching scheme and a point matching scheme. Compared with the standard Fourier modal method, the high order FDMM is more efficient since the matrices in the discretized eigenvalue problems are sparse. Numerical examples are used to illustrated the performance of the method.

1. Introduction

Numerical methods play an important role in the design and optimization of optical and photonic devices. In the last several decades, many numerical methods have been developed for analyzing diffraction gratings [1]. For lamellar gratings or multilayer grating stacks, the modal methods, including the analytic modal method [2–6] and different types of numerical modal methods, are very natural and widely used. For gratings with metal or other lossy materials, the analytic modal method is not so convenient, since it is necessary to find all zeros of a function in the complex plane. The numerical modal methods are easier to use, since the eigenmodes in each grating layer are simply calculated from approximate matrix eigenvalue problems. Depending on how the eigenvalue problems in the grating layers are solved, the numerical modal methods can be classified as the Fourier modal method (FMM) [7–13], the finite difference modal method (FDMM) [14], the B-spline modal method [15, 16], the polynomial expansion modal method [17,18], the pseudospectral modal method [19,20], etc.

For any numerical modal method, it is necessary to solve a matrix eigenvalue problem for each grating layer. Typically, this eigenvalue problem is the most expensive step of the method. In a previous work [21], we developed a Dirichlet-to-Neumann (DtN) map method to replace the matrix eigenvalue problem by some less expensive calculations. However, the DtN map method is only available for gratings in the classical mounting (in-plane diffraction).

Actually, the computation cost of a matrix eigenvalue problem depends on both the size and the structure of the matrix. The eigenvalue problem of a symmetric tridiagonal matrix is much easier to solve than a dense matrix of the same size [22]. For non-symmetric tridiagonal matrices or matrix pairs, there are also a few algorithms that can take advantage of the special matrix structure [23–26]. Among the existing numerical modal methods, the FDMM [14] has the special advantage of producing essentially tridiagonal matrices. So far, only a low order FDMM has been implemented and it is only for the classical mounting [14]. To calculate the eigenmodes of the grating layer, a lower order method requires a larger matrix than a higher order method. In this paper, we develop a high order FDMM for both conical and classical mountings. The resulting eigenvalue problem involves a pair of essentially tridiagonal matrices. Numerical examples indicate that our high order FDMM has better or similar performance as the standard FMM for matrices of the same size, but the matrix eigenvalue problem in our method is much easier to solve.

2. Problem formulation

For diffraction gratings with one periodic direction, we choose a Cartesian coordinate system such that the x axis is the periodic direction, the z axis is parallel to the grating grooves, and the y axis is the normal to the overall structure. In the y direction, the grating is layered where the layers are separated by $0 = y_0 < y_1 < \cdots < y_J = D$ for some positive D, and each layer is y-independent. The structure is described by a z-independent dielectric function $\varepsilon(x, y)$. It satisfies $\varepsilon = \varepsilon^{(1)}$ for $y > D$ and $\varepsilon = \varepsilon^{(2)}$ for $y < 0$, where $\varepsilon^{(1)}$ and $\varepsilon^{(2)}$ are constants. In the region $0 \le y \le D$, $\varepsilon(x, y)$ is periodic in x with period L. For the jth layer given by $y_{j-1} < y < y_j$, we have $\varepsilon = \varepsilon_j(x)$.

For time harmonic electromagnetic waves with the time dependence $\exp(-i\omega t)$, where ω is the angular frequency, the governing equations are the frequency-domain Maxwell's equations:

$$\nabla \times \boldsymbol{E} = ik_0 \boldsymbol{H}, \quad \nabla \times \boldsymbol{H} = -ik_0 \varepsilon \boldsymbol{E}. \tag{1}$$

In the above, $\boldsymbol{E}$ is the electric field, $\boldsymbol{H}$ is the magnetic field multiplied by the free space impedance, and k_0 is the free space wavenumber. In the top region ($y > D$), we specify an incident plane wave with a wave vector $(\alpha_0, -\beta_0^{(1)}, \gamma_0)$ satisfying $\beta_0^{(1)} > 0$ and

$$\alpha_0^2 + [\beta_0^{(1)}]^2 + \gamma_0^2 = k_0^2 \varepsilon^{(1)}. \tag{2}$$

The x component of the electric field of the incident wave is given by

$$E_x^{(i)} = I_x^{(e)} \exp\{i[\alpha_0 x - \beta_0^{(1)}(y - D) + \gamma_0 z]\}, \quad y > D, \tag{3}$$

where $I_x^{(e)}$ is the amplitude of $E_x^{(i)}$. In this paper, we work with the four components E_x, H_x, E_z and H_z. For the incident wave, the amplitudes of $H_x^{(i)}$, $E_z^{(i)}$ and $H_z^{(i)}$ are $I_x^{(h)}$, $I_z^{(e)}$ and

$I_z^{(h)}$, respectively. Since there are only two linearly independent plane waves with the same wave vector, the z components are related to the x components by

$$\begin{bmatrix} I_z^{(e)} \\ I_z^{(h)} \end{bmatrix} = \frac{1}{[\beta_0^{(1)}]^2 + \gamma_0^2} \begin{bmatrix} -\gamma_0\alpha_0 & -k_0\beta_0^{(1)} \\ k_0\varepsilon^{(1)}\beta_0^{(1)} & -\gamma_0\alpha_0 \end{bmatrix} \begin{bmatrix} I_x^{(e)} \\ I_x^{(h)} \end{bmatrix}. \tag{4}$$

Since the structure is periodic in x and the incident wave depends on x as $\exp(i\alpha_0 x)$, the electromagnetic field is quasi-periodic in x, that is

$$\boldsymbol{E}(x+L,y,z) = \gamma \boldsymbol{E}(x,y,z), \quad \boldsymbol{H}(x+L,y,z) = \gamma \boldsymbol{H}(x,y,z), \tag{5}$$

where $\gamma = \exp(i\alpha_0 L)$.

For $y > D$, the total electromagnetic field is the sum of incident and reflected waves. The E_x component of the reflected wave can be written as

$$E_x^{(r)} = \sum_{l=-\infty}^{\infty} R_{x,l}^{(e)} \exp\{i[\alpha_l x + \beta_l^{(1)}(y-D) + \gamma_0 z]\}, \quad y > D, \tag{6}$$

where $\alpha_l = \alpha_0 + 2\pi l/L$, $\beta_l^{(1)} = \left[k_0^2\varepsilon^{(1)} - \alpha_l^2 - \gamma_0^2\right]^{1/2}$, and $R_{x,l}^{(e)}$ are the unknown coefficients. In the bottom region ($y < 0$), the total field is just the transmitted field. The E_x component of the transmitted field can be written as

$$E_x^{(t)} = \sum_{l=-\infty}^{\infty} T_{x,l}^{(e)} \exp\{i[\alpha_l x - \beta_l^{(2)} y + \gamma_0 z]\}, \quad y < 0, \tag{7}$$

where $\beta_l^{(2)} = \left[k_0^2\varepsilon^{(2)} - \alpha_l^2 - \gamma_0^2\right]^{1/2}$ and $T_{x,l}^{(e)}$ are unknown coefficients. For the other three components H_x, E_z and H_z, the unknown coefficients for the reflected and transmitted waves are $R_{x,l}^{(h)}$, $R_{z,l}^{(e)}$, $R_{z,l}^{(h)}$ and $T_{x,l}^{(h)}$, $T_{z,l}^{(e)}$, $T_{z,l}^{(h)}$, respectively. The objective is to calculate the unknown coefficients of the reflected and transmitted waves. Notice that similar to Eq. (4), the coefficients for the z components of the reflected and transmitted waves can be expressed in terms of the coefficients for the x components.

From these coefficients, we can find the diffraction efficiencies. For example, the diffraction efficiency of the lth reflected order is given by

$$\mathrm{DE}_l^{(r)} = \frac{\mathrm{Re}(\beta_l^{(1)})}{\beta_0^{(1)}} \cdot \frac{k_0^2\varepsilon^{(1)} - \alpha_0^2}{k_0^2\varepsilon^{(1)} - \alpha_l^2} \cdot \frac{\varepsilon^{(1)}|R_{x,l}^{(e)}|^2 + |R_{x,l}^{(h)}|^2}{\varepsilon^{(1)}|I_x^{(e)}|^2 + |I_x^{(h)}|^2}. \tag{8}$$

Since the z-dependence is always $\exp(i\gamma_0 z)$, we drop the explicit z-dependence in the following sections.

3. Modal solutions

The modal methods express the electromagnetic field in each y-independent layer by eigenfunction expansions. Consider the jth layer with the dielectric function $\varepsilon_j(x)$. To simplify the notations, we drop the superscript j for ε_j. Since ε depends on x only, the Maxwell's equations (1) can be reduced to

$$\frac{\partial^2 E_x}{\partial y^2} + \frac{\partial}{\partial x}\left[\frac{1}{\varepsilon}\frac{\partial(\varepsilon E_x)}{\partial x}\right] + (k_0^2\varepsilon - \gamma_0^2)E_x = 0, \tag{9}$$

$$\frac{\partial^2 H_x}{\partial y^2} + \frac{\partial^2 H_x}{\partial x^2} + (k_0^2\varepsilon - \gamma_0^2)H_x = 0, \tag{10}$$

$$\left(\gamma_0^2 - \frac{\partial^2}{\partial y^2}\right)E_z = i\frac{\gamma_0}{\varepsilon}\frac{\partial(\varepsilon E_x)}{\partial x} - ik_0\frac{\partial H_x}{\partial y}, \tag{11}$$

$$\left(\gamma_0^2 - \frac{\partial^2}{\partial y^2}\right)H_z = ik_0\varepsilon\frac{\partial E_x}{\partial y} + i\gamma_0\frac{\partial H_x}{\partial x}. \tag{12}$$

Notice that E_x and H_x satisfy independent homogeneous Helmholtz equations, and E_z and H_z are related to E_x and H_x.

The general solutions of Eqs. (9) and (10) can be written down as

$$E_x(x,y) = \sum_{m=1}^{\infty}\phi_m(x)\left[a_m e^{i\mu_m(y-y_{j-1})} + b_m e^{-i\mu_m(y-y_j)}\right], \tag{13}$$

$$H_x(x,y) = \sum_{m=1}^{\infty}\psi_m(x)\left[c_m e^{i\nu_m(y-y_{j-1})} + d_m e^{-i\nu_m(y-y_j)}\right], \tag{14}$$

where a_m, b_m, c_m and d_m are unknown coefficients, $\{\phi_m, \mu_m^2\}$ and $\{\psi_m, \nu_m^2\}$ are eigenpairs for E_x and H_x, respectively. To obtain the eigenvalue problem for E_x, we consider a special solution $\phi(x)e^{\pm i\mu y}$ satisfying Eq. (9) and the quasi-periodic condition (5). We have

$$\frac{d}{dx}\left[\frac{1}{\varepsilon}\frac{d(\varepsilon\phi)}{dx}\right] + (k_0^2\varepsilon - \gamma_0^2)\phi = \mu^2\phi, \quad 0 < x < L, \tag{15}$$

$$\varepsilon(L^-)\phi(L^-) = \gamma\varepsilon(0^+)\phi(0^+), \tag{16}$$

$$\frac{d\phi}{dx}(L^-) = \gamma\frac{d\phi}{dx}(0^+). \tag{17}$$

Similarly, the eigenvalue problem for H_x is

$$\frac{d^2\psi}{dx^2} + (k_0^2\varepsilon - \gamma_0^2)\psi = \nu^2\psi, \quad 0 < x < L, \tag{18}$$

$$\psi(L) = \gamma\psi(0), \tag{19}$$

$$\frac{d\psi}{dx}(L) = \gamma\frac{d\psi}{dx}(0). \tag{20}$$

Using Eqs. (13) and (14), we can easily write down the z components:

$$\begin{aligned} E_z(x,y) &= \sum_{m=1}^{\infty} V_{12,m}(x)\left[a_m e^{i\mu_m(y-y_{j-1})} + b_m e^{-i\mu_m(y-y_j)}\right] \\ &\quad + \sum_{m=1}^{\infty} V_{11,m}(x)\left[c_m e^{i\nu_m(y-y_{j-1})} - d_m e^{-i\nu_m(y-y_j)}\right], \qquad (21) \\ H_z(x,y) &= +\sum_{m=1}^{\infty} V_{22,m}(x)\left[a_m e^{i\mu_m(y-y_{j-1})} - b_m e^{-i\mu_m(y-y_j)}\right] \\ &\quad + \sum_{m=1}^{\infty} V_{21,m}(x)\left[c_m e^{i\nu_m(y-y_{j-1})} + d_m e^{-i\nu_m(y-y_j)}\right], \qquad (22) \end{aligned}$$

where

$$V_{11,m}(x) = \frac{k_0\nu_m}{\gamma_0^2+\nu_m^2}\psi_m(x), \qquad V_{12,m}(x) = \frac{i\gamma_0}{(\gamma_0^2+\mu_m^2)\varepsilon(x)}\frac{d}{dx}\left[\varepsilon(x)\phi_m(x)\right], \qquad (23)$$

$$V_{21,m}(x) = \frac{i\gamma_0}{\gamma_0^2+\nu_m^2}\frac{d\psi_m(x)}{dx}, \qquad V_{22,m}(x) = -\frac{k_0\mu_m\varepsilon(x)}{\gamma_0^2+\mu_m^2}\phi_m(x). \qquad (24)$$

.

For $\tilde{\phi} = \varepsilon\phi$, Eq. (15) becomes

$$\varepsilon\frac{d}{dx}\left(\frac{1}{\varepsilon}\frac{d\tilde{\phi}}{dx}\right) + (k_0^2\varepsilon - \gamma_0^2)\tilde{\phi} = \mu^2\tilde{\phi}, \quad 0 < x < L. \qquad (25)$$

For in-plane diffraction problems, we have $\gamma_0 = 0$, then E_z is only related to H_x, and H_z is only related to E_x. In that case, the eigenvalue problems are usually formulated for E_z and H_z where the governing equations correspond to (18) and (25), respectively.

4. High order finite difference schemes

For a smooth function $f(x)$, the following fourth order finite difference formula is well-known:

$$\frac{1}{h^2}\left[f(x-h) - 2f(x) + f(x+h)\right] = \frac{1}{12}\left[f''(x-h) + 10f''(x) + f''(x+h)\right] + O(h^4), \qquad (26)$$

where the prime is used to denote the derivative with respect to x. In a y-independent layer, if $\varepsilon(x)$ has discontinuities, the eigenfunctions ϕ and ψ are not smooth. If x_* is a discontinuity of ε, then $\varepsilon\phi$, ψ and ψ' are continuous at x_*, ϕ is discontinuous at x_*, but $\phi'(x_*^+) = \phi'(x_*^-)$, where $\phi'(x_*^\pm)$ denote the one-sided limits of ϕ' at x_*. If ε is piecewise constant, the interface conditions for the second and higher order derivatives of ϕ and ψ can be obtained from Eqs. (15) and (18), respectively. In particular, we notice that ϕ'' and ψ'' are discontinuous at x_*, therefore ϕ and ψ are not smooth. In [27], Chiou *et al.* extended formula (26) to non-smooth functions with known interface conditions. The result can be written as

$$a_1 f(x-h) + a_2 f(x) + a_3 f(x+h) \approx b_1 f''(x-h) + b_2 f''(x) + b_3 f(x+h), \qquad (27)$$

where the coefficients a_1, a_2, ..., b_3 depend on the locations of the discontinuities in $(x-h, x+h]$, the interface conditions, and the values of ε in that interval. The coefficients can be scaled to satisfy $b_1+b_2+b_3=1$ and they are reduced to the coefficients in (26) when ε is smooth. A simple procedure for computing these coefficients is given in [21].

Since x or $x\pm h$ may be a discontinuous point of ε, we use one-sided limits for ϕ, ϕ', ϕ'' and ψ'' at x^+ and $(x\pm h)^+$. Since E_z and H_z are related to E_x and H_x by first order derivatives in x, it is convenient to use staggered grids. We choose to discretize ϕ and ϕ'' at the half-integer grid points $x_{p+1/2}=(p+1/2)h$ for $0\le p<N$, where $h=L/N$ is the grid size and N is a given positive integer, and discretize ψ and ψ'' at the integer grid points $x_p=ph$ for $0\le p\le N$. Assuming ε is piecewise constant, at the positive side of the grid point x_p, Eq. (18) becomes

$$\psi''(x_p^+)=-[k_0^2\varepsilon(x_p^+)-\gamma_0^2]\psi(x_p)+\nu^2\psi(x_p). \tag{28}$$

Inserting $\psi''(x_p^+)$ above and similar equations for $\psi''(x_{p+1}^+)$ and $\psi''(x_{p-1}^+)$ into (27) (for $f=\psi$ and $x=x_p^+$), we obtain a linear equation involving $\psi(x_{p-1})$, $\psi(x_p)$, $\psi(x_{p+1})$ and ν^2. Putting such equations for all p together and using the quasi-periodic condition $\psi(x+L)=\gamma\psi(x)$, we obtain a matrix eigenvalue problem

$$\boldsymbol{A}\boldsymbol{\psi}=\nu^2\boldsymbol{B}\boldsymbol{\psi} \tag{29}$$

where $\boldsymbol{\psi}=[\psi(x_1),\psi(x_2),...,\psi(x_N)]^T$, $\boldsymbol{A}$ and $\boldsymbol{B}$ are tridiagonal matrices with extra non-zero $(1,N)$ and $(N,1)$ entries. For simplicity, we call matrices $\boldsymbol{A}$ and $\boldsymbol{B}$ essentially tridiagonal. The eigenvalue problem for ϕ, i.e., Eq. (15), can be discretized similarly.

To write down E_z and H_z in the y-independent layers, we need to evaluate the first order derivatives $\varepsilon^{-1}\partial_x(\varepsilon E_x)$ and $\partial_x H_x$. The standard second order central difference formula

$$f'(x)=\frac{f(x+0.5h)-f(x-0.5h)}{h}+O(h^2) \tag{30}$$

has a fourth order extension

$$\frac{1}{22}f'(x-h)+f'(x)+\frac{1}{22}f'(x+h)=\frac{12}{11h}\left[f(x+0.5h)-f(x-0.5h)\right]+O(h^4). \tag{31}$$

Similar to the case for second order derivatives, we can extend the above formula to

$$c_1f'(x-h)+f'(x)+c_2f'(x+h)\approx d_1f(x-0.5h)+d_2f(x+0.5h), \tag{32}$$

when f has discontinuities in $(x-h,x+h]$ with known interface conditions. The coefficients c_1, c_2, d_1 and d_2 depend on the locations of the discontinuities, the interface conditions and the values of ε. A detailed procedure for calculating these coefficients is given in the appendix. If the discontinuities are located at x, $x\pm h$ or $x\pm 0.5h$, the formula has an $O(h^4)$

error. Applying formula (32) to function ψ at $x = x_{p+1/2}$ for $0 \le p < N$ and using the quasi-periodic condition, we obtain

$$\boldsymbol{C}\boldsymbol{\psi}' = \boldsymbol{D}\boldsymbol{\psi} \tag{33}$$

where $\boldsymbol{\psi}$ is given earlier, $\boldsymbol{\psi}' = [\psi'(x_{1/2}), \psi'(x_{3/2}), ..., \psi'(x_{N-1/2})]^T$, $\boldsymbol{C}$ is an essentially tridiagonal matrix, and $\boldsymbol{D}$ is a bidiagonal matrix with an extra non-zero $(1, N)$ entry. The first order derivative for ϕ can be obtained similarly.

5. Interface conditions

With the modal expansions in the y-independent layers and the Rayleigh expansions (6) and (7) in the top and bottom regions, we can set up a linear system for all unknown coefficients by imposing the continuities of E_x, H_x, E_z and H_z at the interfaces between the layers. To distinguish the solutions in different layers, we add a subscript (j) to all quantities in the jth layer given by $y_{j-1} < y < y_j$. Therefore, the eigenvalues, the eigenfunctions and the unknown coefficients in the jth layer are $\mu_m^{(j)}$ and $\nu_m^{(j)}$, $\phi_m^{(j)}$ and $\psi_m^{(j)}$, $a_m^{(j)}$, $b_m^{(j)}$, $c_m^{(j)}$ and $d_m^{(j)}$, respectively.

Following the discretization for one period of x, i.e., $0 \le x \le L$, with N integer grid points and N half-integer grid points, it is natural to impose the interface conditions by point matching. For example, the continuity of H_x at the interface $y = y_j$ (for $0 < j < J$) can be written as

$$\sum_{m=1}^{N} \psi_m^{(j)}(x_p) \left[c_m^{(j)} e^{i\nu_m^{(j)}(y_j - y_{j-1})} + d_m^{(j)} \right] = \sum_{m=1}^{N} \psi_m^{(j+1)}(x_p) \left[c_m^{(j+1)} + d_m^{(j+1)} e^{i\nu_m^{(j+1)}(y_{j+1} - y_j)} \right]$$

for $1 \le p \le N$. The continuities of E_x, E_z and H_z can be similarly written down. Notice that E_x and H_z are evaluated at the half-integer grid points, but E_z is evaluated at the integer grid points. The interface conditions at $y_J = D$ and $y_0 = 0$ provide the link with the field in the top and bottom regions, where the Rayleigh expansions are truncated to N terms given by $-N/2 \le l < N/2$ if N is even or $-(N-1)/2 \le l \le (N-1)/2$ if N is odd. All these conditions lead to a linear system with a $4N(J+1) \times 4N(J+1)$ coefficient matrix. The $4N(J+1)$ unknowns are $a_m^{(j)}$, $b_m^{(j)}$, $c_m^{(j)}$ and $d_m^{(j)}$ for $1 \le m \le N$ and $1 \le j \le J$, and $R_{x,l}^{(e)}$, $R_{x,l}^{(h)}$, $T_{x,l}^{(e)}$ and $T_{x,l}^{(h)}$ for the above range of l. The right hand side of this linear system is related to the amplitudes of the incident wave $I_x^{(e)}$ and $I_x^{(h)}$. We call this method the point-matching finite difference modal method (FDMM(p)).

Since not all numerical eigenmodes are good approximations of the true eigenmodes of the y-independent layers, it is often beneficial to retain only the first M modes for some $M < N$. For that purpose, we order the eigenvalues $[\mu_m^{(j)}]^2$ and $[\nu_m^{(j)}]^2$ such that their real parts decrease as m is increased, then the eigenmode expansions in the jth layer are truncated to the first

M terms. For example, E_x is given by

$$E_x(x,y) \approx \sum_{m=1}^{M} \phi_m^{(j)}(x) \left[a_m^{(j)} e^{i\mu_m^{(j)}(y-y_{j-1})} + b_m^{(j)} e^{-i\mu_m^{(j)}(y-y_j)} \right], \quad y_{j-1} < y < y_j, \tag{34}$$

where $\phi_m^{(j)}$ is actually only available at the half-integer grid points $x_{p+1/2}$ for $0 \le p \le N-1$. Meanwhile, the interface conditions can be implemented by matching the first K Fourier coefficients. For E_x, this leads to

$$\int_0^L \left[E_x(x, y_j^+) - E_x(x, y_j^-) \right] e^{-i\alpha_l x} dx = 0, \quad -\frac{K}{2} \le l \le \frac{K}{2} - 1$$

if K is an even integer, or $-(K-1)/2 \le l \le (K-1)/2$ if K is odd. The above is approximately evaluated using E_x given in (34) and a similar expansion in the $(j+1)$th layer, and a numerical integration based on the N half-integer grid points. The numerical integrations are used to evaluate

$$\int_0^L \phi_m^{(j)}(x) e^{-i\alpha_l x} dx$$

for $1 \le m \le M$, $1 \le j \le J$ and K different values of l. For $E_x(x, y_0^-)$ and $E_x(x, y_J^+)$, the integrals are evaluated analytically. Notice that the integer K satisfies $M \le K \le N$. If $K = M$, this process leads to a linear system with a square coefficient matrix for $4M(J+1)$ unknowns. If $K > M$, we obtain $4K(J+1)$ equations for $4(MJ+K)$ unknowns: $\{a_m^{(j)}, b_m^{(j)}, c_m^{(j)}, d_m^{(j)}\}$ for $1 \le m \le M$ and $1 \le j \le J$, and $\{R_{x,l}^{(e)}, R_{x,l}^{(h)}, T_{x,l}^{(e)}, T_{x,l}^{(h)}\}$ for K different values of l. In that case, the problem is solved by a least squares method. We call this Fourier-matching finite difference modal method (FDMM(f)). Notice that the method approximates an analytic modal method if $K = M$ and N is much larger than M.

6. Numerical examples

In this section, we illustrate our method by a few numerical examples. The first example is a metallic grating shown in Fig. 1(a), where the dielectric constant of the metal is $\varepsilon^{(2)} = (0.22 + 6.71i)^2$. The structure has been analyzed previously by many authors [10, 20]. We consider the classical mounting where $\gamma_0 = 0$, and assume that the incident plane wave has a 30° incident angle with the y axis and a free space wavelength $\lambda = 1\,\mu$m. For the transverse electric (TE) polarization, the FMM and the two FDMM versions have similar performance. The transverse magnetic (TM) polarization is more challenging. In Table 1, we show the computed diffraction efficiency of the zeroth reflected order by the standard FMM, the FDMM(p) and the FDMM(f). The integer N in the first column denotes the number of grid points for discretizing x or the total number of retained Fourier coefficients in the FMM. For the FDMM(f), we choose $M = 5N/6$ and $K = N$ so that the problem is solved by the least squares method. From an earlier work [20], we know that the exact value (up

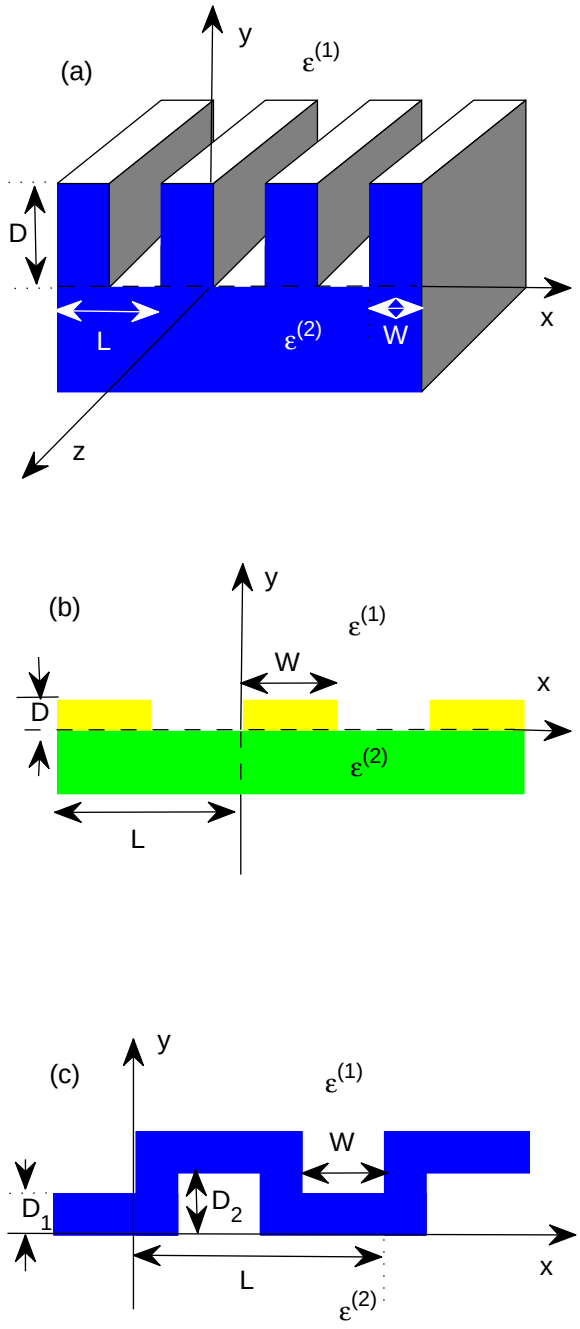

Fig. 1. (a) A simple lamellar grating with $L = 1\,\mu$m, $D = L$, $W = L/2$ and $\varepsilon^{(1)} = 1$; (b) Parallel gold strips with $L = 0.4\,\mu$m, $D = L/8$, $W = L/2$ and $\varepsilon^{(1)} = 1$; (c) A silver meander of width $D_1 = 30\,$nm, with $D_2 = 40\,$nm and $W = L/2 - D_1$.

Table 1. Metallic lamellar grating (lossy): diffraction efficiency of the zeroth reflected order for the TM polarization.

N	FMM	FDMM(p)	FDMM(f)
120	0.84759	0.848544	0.848131
168	0.84783	0.848523	0.848344
240	0.84804	0.848508	0.848439
312	0.84816	0.848500	0.848468
360	0.84821	0.848497	0.848477
408	0.84825	0.848495	0.848481
456	0.84828	0.848493	0.848484

to the first 6 digits) is 0.848484. Therefore, the FDMM(f) is clearly more accurate than the other two methods. For example, if $N = 360$, the FDMM(f), the FDMM(p) and the FMM give 5, 4 and 3 correct digits, respectively.

Next, we follow previous works [14,20] and modify this example by assuming that the metal is lossless, so that $\varepsilon^{(2)} = -6.71^2$. Again, the TE case is relatively simple. In Table 2, we list

Table 2. Metallic lamellar grating (lossless): diffraction efficiency of the zeroth reflected order for the TM polarization.

N	FMM	FDMM(f)
240	0.8930	0.892911
360	0.8930	0.892961
432	0.8931	0.892971
456	0.8932	0.892973
480	0.8931	0.892974

the numerical results for the TM polarization obtained by the FMM and the FDMM(f). It is clear that the FDMM(f) gives more accurate results than the FMM. For $N = 432$, the FDMM(f) gives 5 correct digits (0.89297), while FMM has only three correct digits.

The second example is a gold grating shown in Fig. 1(b). It is similar to a structure analyzed by Liu *et al.* [28]. The dielectric constants of the top and bottom media are $\varepsilon^{(1)} = 1$ and $\varepsilon^{(2)} = 1.45^2$, respectively. Using the refractive index of gold given in [29], we calculate the transmission spectra (diffraction efficiencies of the zeroth transmitted order as functions

of the wavelength) for both TE and TM polarizations and for three different incident angles. The results obtained by the FMM and the FDMM(f) are shown in Fig. 6. The convergence

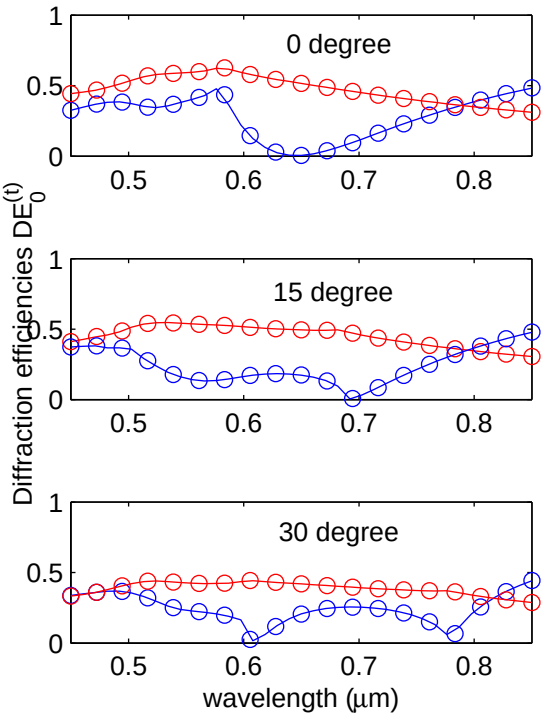

Fig. 2. Transmission spectra of the gold grating for incident waves in TE (red) and TM (blue) polarizations, calculated by the FMM (circles) and FDMM(f) (solid lines).

of the numerical solutions is carefully checked for the normal incidence and for the free space wavelength $\lambda = 0.75\,\mu$m. As in the previous example, the TE case is relatively simple and both methods give satisfactory results. For the TM case, the FDMM(f) solutions are obtained using $M = 5N/12$ and $K = N$, and they agree well with the FMM results.

The third example is a silver meander shown in Fig. 1(c). It was originally proposed and analyzed by Fu *et al.* [30]. Both top and bottom media are air, thus, $\varepsilon^{(1)} = \varepsilon^{(2)} = 1$. The period in the x direction is either $L = 200\,$nm or $L = 400\,$nm. To use a modal method, it is necessary to divide this structure into three y-independent layers with $y_0 = 0$, $y_1 = D_1 = 30\,$nm, $y_2 = D_2 = 40\,$nm and $y_3 = D_1 + D_2 = D = 70\,$nm. For this structure, we use the refractive index of silver given in [29], consider a normal incident wave for the TM polarization, and calculate the transmission and reflection spectra (diffraction efficiencies of

the zeroth transmitted and reflected orders) using both the FMM and the FDMM(f). The results are plotted in Fig. 3. If we use the Drude model for silver as in [30], the results

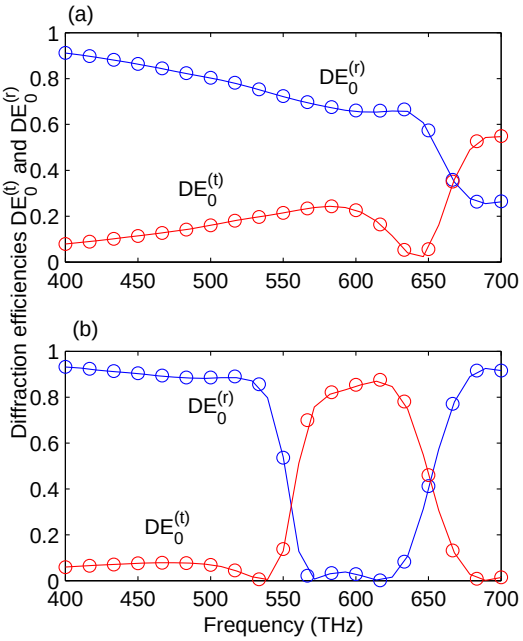

Fig. 3. Transmission and reflection spectra of the silver meander calculated by the FMM (circles) and the FDMM(f) (solid lines). Figures (a) and (b) correspond to $L = 200\,\text{nm}$ and $L = 400\text{nm}$, respectively.

are somewhat different. To test the convergence, we fix the frequency of the incident wave at $f = 600\,\text{THz}$, and calculate the diffraction efficiency of the zeroth transmitted order by the FMM and the FDMM(f). The results are shown in Table 3. For the FDMM(f), we use $M = K = N$. It is clear that the FDMM(f) has a better convergence. Notice that the FDMM(f) gives four correct digits (0.8539) for $N = 200$, while the FMM has only two correct digits for $N = 400$.

Finally, we consider a metallic grating in a conical mounting. The problem was previously analyzed by Li using an analytic modal method [4]. The structure is identical to the one shown in Fig. 1(a), but the dielectric constant of the metal is assumed to be $\varepsilon^{(2)} = (0.1 + 5.0i)^2$. Furthermore, we choose an incident wave with a free space wavelength $\lambda = 0.5\,\mu\text{m}$, a wave vector $(\alpha_0, -\beta_0^{(1)}, \gamma_0) = k_0(\sqrt{2}/4, -\sqrt{3}/2, \sqrt{2}/4)$ and amplitudes $I_x^{(e)} = 2 - \sqrt{3}$ and $I_x^{(h)} = 2 + \sqrt{3}$. For this problem, there are four propagating reflected diffraction orders. In Table 4, we compare the diffraction efficiency of the zeroth reflected order computed by the FMM and the FDMM(f). For the FDMM(f), we use $M = 2N/3$ and $K = N$. For this

Table 3. Silver meander: diffraction efficiency of the zeroth transmitted order for a normal incident wave in the TM polarization.

N	FMM	FDMM(f)
80	0.81636	0.853363
120	0.84350	0.853658
160	0.84735	0.853791
200	0.84576	0.853864
240	0.84845	0.853911
280	0.84896	0.853942
320	0.84943	0.853965
360	0.85022	0.853982
400	0.85105	0.853996

problem, an accurate solution was previously obtained by the boundary integral equation Neumann-to-Dirichlet map (BIE-NtD) method [31]. The "exact" solution with 5 correct digits should be 0.44158. The results in Table 4 indicate that for this example, the FMM is more accurate than the FDMM(f). Notice that the FMM gives a good result for $N = 300$, but it shows little improvement when N is further increased.

7. Conclusion

In the previous sections, we developed a high order FDMM for both conical and classical mountings. When the eigenvalue problems in a grating layer is discretized, the FDMM produces matrix eigenvalue problems involving essentially tridiagonal matrices, while other numerical modal methods give rise to dense matrices. This implies that when the size of the matrices is fixed, the matrix eigenvalue problems in a FDMM can be solved more efficiently using special numerical methods that take advantage of the matrix structures [23–26]. Compared with a previous FDMM [14], the high order FDMM developed in this paper gives more accurate approximations to the eigenmodes in each y-independent layer, but the overall performance of the method depends more on the behavior of the electromagnetic field at the corners. In particular, for conical diffractions, E_x could be infinity at the corners. In that case, the Rayleigh expansions (6) and (7), and eigenfunction expansions (13) can only have a very slow convergence. For the interface conditions between the y-independent layers, we implemented two schemes and observed that the Fourier matching scheme is more accurate than the point matching scheme. In particular, we do not use all numerical eigenmodes to expand the field in the grating layers, since some of these modes are not good approximations

Table 4. Metallic lamellar grating in a conical mounting: diffraction efficiency of the zeroth reflected order.

N	FMM	FDMM(f)
96	0.441907	0.44083
192	0.441605	0.44133
300	0.441572	0.44144
384	0.441566	0.44148
492	0.441567	0.44151
600	0.441570	0.44153
768	0.441573	0.44156

to the true eigenmodes.

We have compared the accuracy of our FDMM with the standard version of the FMM, assuming that the matrices in the discretized eigenvalue problems have the same size. Our method performs better than the FMM except for the last example. The performance of the FMM can be improved by the adaptive spatial resolution technique [10]. This technique may be applicable to other numerical modal methods, such as the FDMM developed in this paper, but it is not very convenient for structures with multiple discontinuities in ε.

Appendix

To derive high order finite difference formulas (27) and (32) on intervals containing a discontinuity x_* where the function f or its derivatives may be discontinuous, we need the matching conditions at x_* given in a matrix J such that

$$\Phi(x_*^+) = \boldsymbol{J}\Phi(x_*^-),$$

where $\Phi(x) = \left[f(x), f'(x), f''(x), ..., f^{(5)}(x)\right]^T$. We assume that the inverse of J is also known explicitly. For ϕ satisfying (15) and assuming ε is piecewise constant, we have

$$\boldsymbol{J} = \begin{bmatrix} \rho & & & & & \\ 0 & 1 & & & & \\ \eta\rho & 0 & \rho & & & \\ 0 & \eta & 0 & 1 & & \\ \eta^2\rho & 0 & 2\eta\rho & 0 & \rho & \\ 0 & \eta^2 & 0 & 2\eta & 0 & 1 \end{bmatrix}, \quad \boldsymbol{J}^{-1} = \begin{bmatrix} 1/\rho & & & & & \\ 0 & 1 & & & & \\ -\eta/\rho & 0 & 1/\rho & & & \\ 0 & -\eta & 0 & 1 & & \\ \eta^2/\rho & 0 & -2\eta/\rho & 0 & 1/\rho & \\ 0 & \eta^2 & 0 & -2\eta & 0 & 1 \end{bmatrix},$$

where $\eta = k_0^2[\varepsilon(x_*^-) - \varepsilon(x_*^+)]$ and $\rho = \varepsilon(x_*^-)/\varepsilon(x_*^+)$. To obtain the above result, we notice that $\varepsilon\phi$ and ϕ' are continuous at x_*, and use equation (15) to find the conditions for the

higher order derivatives. For function ψ satisfying (18), a different $\boldsymbol{J}$ can be easily obtained.

Assuming $x-h < x_* \le x+h$, and using Taylor expansions and the matching conditions at x_*, we can find the coefficients c_{jk} (for $1 \le j \le 4$ and $0 \le k \le 5$) such that

$$\begin{aligned}
f'((x-h)^+) &= [c_{10},\ c_{11},\ c_{12},\ c_{13},\ c_{14},\ c_{15}]\,\Phi(x^+) + O(h^5),\\
f'((x+h)^+) &= [c_{20},\ c_{21},\ c_{22},\ c_{23},\ c_{24},\ c_{25}]\,\Phi(x^+) + O(h^5),\\
f((x-0.5h)^+) &= [c_{30},\ c_{31},\ c_{32},\ c_{33},\ c_{34},\ c_{35}]\,\Phi(x^+) + O(h^6),\\
f((x+0.5h)^+) &= [c_{40},\ c_{41},\ c_{42},\ c_{43},\ c_{44},\ c_{45}]\,\Phi(x^+) + O(h^6).
\end{aligned}$$

The coefficients c_1, c_2, d_1 and d_2 in (32) can be found by eliminating $f(x^+)$, $f'(x^+)$, $f''(x^+)$ and $f'''(x^+)$. This leads to the following system of equations

$$\begin{bmatrix} c_{10} & c_{20} & c_{30} & c_{40} \\ c_{11} & c_{21} & c_{31} & c_{41} \\ c_{12} & c_{22} & c_{32} & c_{42} \\ c_{13} & c_{23} & c_{33} & c_{43} \end{bmatrix} \begin{bmatrix} -c_1 \\ -c_2 \\ d_1 \\ d_2 \end{bmatrix} = \begin{bmatrix} 0 \\ 1 \\ 0 \\ 0 \end{bmatrix}.$$

For the second order derivative formula (27), a procedure for calculating the coefficients is given in [21].

Acknowledgments

This research was partially supported by a grant from the Research Grants Council of Hong Kong Special Administrative Region, China (Project No. CityU 102008).

References

1. R. Petit, *Electromagnetic Theory of Gratings*, Springer-Verlag, Berlin, (1980).
2. L. C. Botten, M. S. Craig, R. C. McPhedran, J. L. Adams, and J. R. Andrewartha, "The dielectric lamellar diffraction grating," Optica Acta **28**, 413-428 (1981).
3. S. T. Peng, "Rigorous formulation of scattering and guidance by dielectric grating waveguides: general case of oblique incidence", J. Opt. Soc. Am. A **6** 1869-1883 (1989).
4. L. Li, "A modal analysis of lamellar diffraction gratings in conical mountings", J. Mod. Opt. **40**, 553-573 (1993).
5. M. Foresti, L. Menez, and A. V. Tishchenko, "Modal method in deep metal-dielectric gratings: the decisive role of hidden modes," J. Opt. Soc. Am. A **23**, 2501-2509 (2006).
6. S. Campbell, L. C. Botten, R. C. McPhedran, and C. M. de Sterke, "Modal method for classical diffraction by slanted lamellar gratings," J. Opt. Soc. Am. A **25**, 2415-2426 (2008).
7. P. Lalanne and G. M. Morris, "Highly improved convergence of the coupled-wave method for TM polarization", J. Opt. Soc. Am. A **13**, 779-784 (1996).

8. G. Granet and B. Guizal, "Efficient implementation of the coupled-wave method for metallic lamellar gratings in TM polarization", J. Opt. Soc. Am. A **13**, 1019-1023 (1996).
9. L. Li, "Use of Fourier series in the analysis of discontinuous periodic structures", J. Opt. Soc. Am. A **13**, 1870-1876 (1996).
10. G. Granet, "Reformulation of the lamellar grating problem through the concept of adaptive spatial resolution", J. Opt. Soc. Am. A **16**, 2510-2516 (1999).
11. N. M. Lyndin, O. Parriaux, and A. V. Tishchenko, "Modal analysis and suppression of the Fourier modal method instabilities in highly conductive gratings," J. Opt. Soc. Am. A **24**, 3781-3788 (2007).
12. I. Gushchin and A. V. Tishchenko, "Fourier modal method for relief gratings with oblique boundary conditions," J. Opt. Soc. Am. A **27**, 1575-1583 (2010).
13. K. M. Gundu and A. Mafi, "Reliable computation of scattering from metallic binary gratings using Fourier-based modal methods," J. Opt. Soc. Am. A **27**, 1694-1700 (2010).
14. P. Lalanne and J. P. Hugonin, "Numerical performance of finite-difference modal methods for the electromagnetic analysis of one-dimensional lamellar gratings," J. Opt. Soc. Am. A **17**, 1033-1042 (2000).
15. K. Edee, P. Schiavone, and G. Granet, "Analysis of defect in extreme UV lithography mask using a modal method based on nodal B-spline expansion," Japanese Journal of Applied Physics, Part 1 **44**, 6458-6462 (2005).
16. G. Granet, L. B. Andriamanampisoa, K. Raniriharinosy, A. M. Armeanu, and K. Edee, "Modal analysis of lamellar gratings using the moment method with subsectional basis and adaptive spatial resolution," J. Opt. Soc. Am. A **27**, 1303-1310 (2010).
17. R. H. Morf, "Exponentially convergent and numerically efficient solution of Maxwell's equations for lamellar gratings," J. Opt. Soc. Am. A **12**, 1043-1056 (1995).
18. K. Edee, "Modal method based on subsectional Gegenbauer polynomial expansion for lamellar gratings," J. Opt. Soc. Am. A **28**, 2006-2013 (2011).
19. Y.-P. Chiou, W.-L. Yeh, and N.-Y. Shih, "Analysis of highly conducting lamellar gratings with multidomain pseudospectral method," J. Lightwave Technol. **27**, 5151-5159 (2009).
20. D. Song, L. Yuan, and Y. Y. Lu, "Fourier-matching pseudospectral modal method for diffraction gratings," J. Opt. Soc. Am. A **28**, 613-620 (2011).
21. D. Song and Y. Y. Lu, "Chebyshev collocation Dirichlet-to-Neumann map method for diffraction gratings," J. Opt. Soc. Am. A **26**, 1980-1988 (2009).
22. G. H. Golub and C. F. Van Loan, Matrix computations, 3rd ed., Johns Hopkins University Press, 1996.
23. H. Rutishause, "Solution of eigenvalue problems with the LR-transformation," Nat. Bur. Standards Appl. Math. Ser., **49**, 47-81 (1958).
24. A. Bunsegerstner, "An analysis of the HR algorithm for computing the eigenvalues of a

matrix," Linear Algebra Appl., **35**, 155-173 (1981).

25. M. A. Brebner and J. Grad, "Eigenvalues of $Ax = \lambda Bx$ for real symmetric matrices A and B computed by reduction to a pseudosymmetric form and the HR process," Linear Algebra Appl., **43**, 99-118 (1982).
26. D. A. Bini, L. Gemignani, and F. Tisseur, "The Ehrlich-Aberth method for the nonsymmetric tridiagonal eigenvalue problem," SIAM Journal on Matrix Analysis and Applications, **27**, 153-175 (2005).
27. Y. P. Chiou, Y. C. Chiang, and H. C. Chang, "Improved three-point formulas considering the interface conditions in the finite-difference analysis of step-index optical devices", J. Lightwave. Technol. **18**, 243-251 (2000).
28. Z. Liu, K. P. Chen, X. Ni, V. P. Drachev, V. M. Shalaev and A. V. Kildishev, "Experimental verification of two-dimensional spatial harmonic analysis at oblique light incidence," J. Opt. Soc. Am. B **27**, 2465-2470 (2010).
29. P. B. Johnson and R. W. Christy, "Optical Constants of the Noble Metals," Physical Review B **6**, 4370-4379 (1972).
30. L. Fu, H. Schweizer, T. Weiss and H. Giessen, "Optical properties of metallic meanders," J. Opt. Soc. Am. B **26**, B111-B119 (2009).
31. Y. Wu and Y. Y. Lu, "Boundary integral equation Neumann-to-Dirichlet map method for gratings in conical diffraction," J. Opt. Soc. Am. A **28**, 1191-1196 (2011).